2.F Novel Gas Target For Use in Laser Harmonic Generation

Generation of high-order harmonics from laser-atom interactions is complicated because it involves both the single-atom response to the driving laser field and the collective-atom enhancement or deterioration of the signal caused by the phase matching of the emitted harmonic light. Much theoretical work has been done toward understanding the single-atom, harmonic-generation reaction, and phase-matching effects are understood in principle.[1] Experimental work in this field has shown good agreement with theory;[2,3] however, a number of unanswered questions remain. To interpret the experimental results, both the laser and gas distribution must be well characterized. The gas-distribution geometry strongly affects the production of the harmonic light. For physical interest, the distribution of the gas ideally would be as narrow and as low density as possible to reduce the role of phase matching so that the single-atom response in harmonic generation is more apparent. This is particularly true if free electrons are created by ionization during the interaction. In the case of free electrons, a severe phase mismatching can occur if the gas pressure is too high, i.e., 1-μm light traveling 1 mm through free electrons at 10 Torr will undergo a phase shift that is equal to a phase shift of 7π for the 21st harmonic.

High-order, harmonic-generation experiments traditionally have been carried out by focusing a laser into a gas jet.[1–5] The gas jet relies on the principles of fluid flow to propel gas from its orifice in a thin stream where the laser can intersect with the narrow distribution of gas. Lompré *et al.*[6] measured the characteristics of such a gas jet. They were able to produce a 1-mm gas distribution with a peak pressure of 25 Torr. A gas jet must operate at a sufficiently high pressure to ensure a narrow stream of flow. Typically the backing pressure of the jet is hundreds of torr while the usable region of the jet is of the order of tens of torr. A lower pressure causes a more diffuse gas distribution in the plume, making the phase matching in the experiment more difficult.[1] In any case, the density of the gas expelled from a jet varies as a function of distance from the orifice, the distribution becoming broader as the distance increases. This can make the systematic alignment of the intersection between the laser and the gas jet a somewhat difficult and tedious task.

Details of a gas target designed to create well-characterized, narrow gas distributions at low densities (1–2 Torr or less with backing pressures up to 5–10 Torr) are presented. This low-density regime is desirable to reduce the phase-matching effects during the harmonic generation.[1] Also, the low backing pressure has the advantage of reducing the possibility of dimer formation in gases such as Xe.[6] High-order, harmonic-generation results using this target are described in the previous article in this volume.

The gas target is a small cylindrical hole through which the focused laser passes and inside of which gas enters from the middle. Because the laser beam goes through the target, the alignment of the device is comparatively simple. The gas target operates on the principle of molecular flow instead of the principle of

fluid flow, as does the gas jet. Since the flow rate is relatively low, the target can be operated in a continuous rather than a pulsed mode. The density of the gas within the hole remains relatively high while the gas outside the hole disperses quickly (inverse square of the distance from the hole edge). The target operation is limited to low densities just as the gas jet is limited to high densities. If the gas in the target hole is at too high a pressure, plumes may develop out its ends that would lie on top of the incoming and outgoing laser beam. The jet and the target are thus complementary in the sense that they operate in opposite ranges of pressure.

The gas distribution in the target is characterized experimentally. It is perhaps more difficult to characterize than the jet since the gas densities are much lower, and the off-axis line of sight to the interaction region is obstructed by the target itself. However, the gas-density profile can be measured in the region just inside the target opening and outward. There is good agreement between the measurement and a calculation of the gas distribution using a Monte Carlo computer simulation of free molecular flow. The same calculation also predicts the gas-flow rate from the target. The flow rate has been measured for two gas-target designs. In both cases, there is good agreement between the predicted and the measured gas-flow rates.

Gas-Target Design

The gas target consists of two identically machined, cylindrical aluminum pieces glued together with a thin layer of vacuum epoxy. Aluminum is chosen because of its ease of machining. Figure 54.26(a) shows a cut-away portion of the two pieces (upper and lower) already attached around the outer rim. Figure 54.26(b) shows the inside of a single piece so that the cylindrical symmetry is observable. Gas flows from the outer ring-shaped pocket into the gap between the thinly spaced plates and toward the hole at the center. The gas then escapes out both ends of the hole. When gluing the pieces together, the drill bit that made the holes is inserted through both pieces to ensure alignment. As shown in Fig. 54.26, a is the separation of the plates, c is the thickness of the plates, d is the hole diameter, and L is the length from the hole center to the inside edge of the outer gas pocket. Typical values for these are $a = 0.2$ mm, $c = 0.4$ mm, $d = 0.5$ mm, and $L = 4$ mm.

Molecular-Flow Range

A gas that flows within a boundary such as a pipe or some other confining shape is in the molecular-flow range if the collisional mean free path of the particles is longer than the characteristic dimension of the boundary, such as a pipe diameter. Knudsen's number (Kn) is the ratio of a gas particle's collisional mean free path to a typical dimension of the boundary. Pure molecular flow begins when $\mathrm{Kn} > 1$. This regime of gas flow is the best understood. The flow of gas in this range is completely determined by the geometry of the walls and can be calculated numerically using a Monte Carlo averaging technique.[7,8] The standard assumption is that a gas particle travels in a straight path until encountering a wall, where it is re-emitted at some new angle. Because of the molecular coarseness of almost any surface, the new direction of the particle has virtually no correlation with the incident direction. Therefore, when the particle strikes a surface, it is as likely to go back toward where it came from as it is to

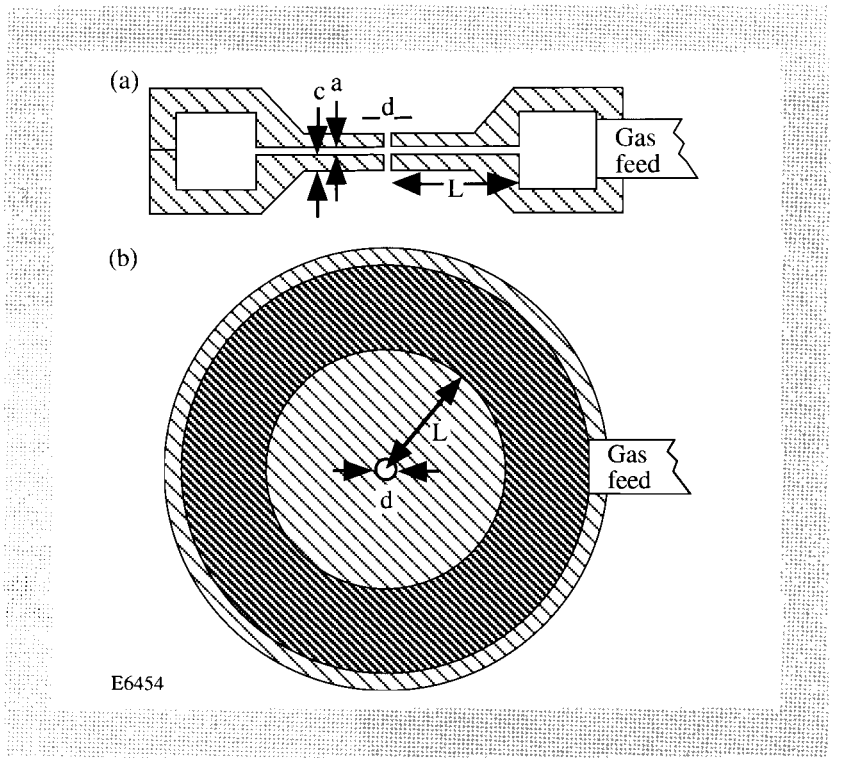

Fig. 54.26
(a) A cutaway view of the two cylindrical gas-target pieces glued together at their outer rims. Gas is fed into the outer ring-shaped pocket. (b) An inside view of a single gas-target piece showing the ring-shaped pocket from which the gas flows across the thin plate toward the center hole.

continue forward through the system. The distribution of the rebound is generally taken to go as the cosine to the surface normal. This assumption has been experimentally verified for various geometries.[8] The problem is usually treated in terms of throughput; that is, for a given system, how likely is a particle that enters one end of the system to emerge out the other end? Harmonic-generation experiments often employ the noble gases. The room-temperature mean free paths of the lighter noble gases are 2 mm, 1 mm, 0.8 mm, 0.6 mm, and 0.4 mm for He, Ne, Ar, Kr, and Xe, respectively, at 0.1-Torr pressure.[8] For the purposes of this article, these numbers should be compared with the typical dimension of the gas-target center (0.5 mm). The mean free path scales inversely with pressure.

The fluid flow regime begins when Kn < 0.01. The flow of the gas in this range behaves very differently from molecular flow. In the fluid flow regime the intraparticle collisions rather than particle-wall collisions dominate the flow of the gas. The regime in between fluid and molecular flow is not well understood. In this case both types of collisions have importance; however, if the value of Kn is nearer to one or the other of the flow ranges, the properties of the flow should be qualitatively similar. Therefore, it is likely that much of the dispersive nature of molecular gas flow is preserved even with Kn as low as 0.1.

Calculation of Trajectories in a Monte Carlo Simulation

This section describes the details necessary for numerically simulating molecular flow through the target. The particles are assumed to move in straight lines between encounters with the target walls. Intraparticle collisions are ignored. Particles enter the region between the thinly spaced plates of the target from the ring-shaped gas pocket at a distance L from the center [refer to Fig. 54.26 throughout this section]. When particles hit the target walls, they rebound in

some new direction, and their trajectory paths are recorded. Each particle propagates until it either exits the target opening or returns to the ring-shaped gas pocket.

The various straight segments of a particle's trajectory are represented by equations of straight lines. The more natural coordinate system for straight lines is Cartesian, wherein the equations for a straight line in three dimensions can be written as $x = m_x z + b_x$ and $y = m_y z + b_y$. The azimuthal symmetry of the target also requires the use of cylindrical coordinates, which are obtained with the transformations $r = \sqrt{x^2 + y^2}$ and $\phi = \tan^{-1}(y/x)$, where $\phi \rightarrow \phi + \pi$ if $x < 0$. The z axis is chosen to lie along the target axis of symmetry, and the origin is taken to be the target center. When the particle encounters the planar surface of the interior of one of the thinly spaced plates, the position of impact is found from $z' = \pm a/2$. The standard assumption at this point is that the particle leaves the surface with a Lambertian distribution.[8] This is the same distribution as produced by an ideal gas escaping from a small hole in a thin-walled container. Under the diffuse-rebound assumption, the slopes for the new line emerging from the point on the planar surface are given by

$$m'_x = \tan\alpha\cos\beta \quad \text{and} \quad m'_y = \tan\alpha\sin\beta\,, \tag{1}$$

where α and β are given by $\alpha = \sin^{-1}(Rnd_1)$ and $\beta = 2\pi(Rnd_2)$. Rnd_1 and Rnd_2 indicate two independent random numbers that have values between 0 and 1. The new z-plane intercepts are calculated by

$$b'_x = b_x + (m_x - m'_x)z' \quad \text{and} \quad b'_y = b_y + (m_y - m'_y)z'\,. \tag{2}$$

This completes the cycle, and the equations for the new particle flight path are defined. These are then used to find the next point of impact with the target wall.

A collision of the particle with the interior of the target's cylindrical hole is more complicated. The z-value at the point of impact is given by

$$z' = \frac{-(m_x b_x + m_y b_y) \pm \sqrt{(m_x b_x + m_y b_y)^2 - (m_x^2 + m_y^2)(b_x^2 + b_y^2 - (d/2)^2)}}{m_x^2 + m_y^2}\,; \tag{3}$$

recall that d is the hole diameter. The azimuthal coordinate of the point of impact is

$$\phi = \tan^{-1}\frac{m_y z' + b_y}{m_x z' + b_x}, \quad \text{where} \quad \phi \rightarrow \phi + \pi \quad \text{if} \quad m_x z' + b_x < 0\,. \tag{4}$$

The slopes for the new line emerging from this point under the diffusive rebound assumption is calculated by

$$m'_x = \frac{\sin\phi\tan\alpha\cos\beta - \cos\phi}{\tan\alpha\sin\beta} \quad \text{and} \quad m'_y = -\frac{\cos\phi\tan\alpha\cos\beta + \sin\phi}{\tan\alpha\sin\beta}\,, \tag{5}$$

where α and β are given the same as before, following Eq. (1). Again, the new z-plane intercepts are calculated by Eq. (2), and the cycle is complete. The trajectory for the particle leaving the point of impact is defined, and the process can be repeated.

The initial position for a particle's trajectory is at the inside edge of the ring-shaped pocket at $r = L$, where the gas density is assumed to be known. The direction of the initial path is distributed randomly over the half-sphere that points toward the target center. The slopes for this path are calculated by Eq. (5) but with $\alpha = \cos^{-1}(Rnd_1)$. Because of azimuthal symmetry it is not essential to randomly choose ϕ, but for conceptual completeness we take $\phi = 2\pi Rnd_3$. The starting z-position is given by $z_o = a(Rnd_4 - 1/2)$, and the z-plane intercepts are determined by $b_x = L\cos\phi - m_x z_o$ and $b_y = L\sin\phi - m_y z_o$. Each particle propagates from the input position until it either goes out the target hole or returns to the ring-shaped gas pocket at radius L. The flow rate of the particles can be determined from the ratio of the number of particles that successfully exit the target to the total number of trial particles. The density of the gas as a function of position is obtained by summing over the intersections of all the particle trajectories with each elemental volume of the target.

Fig. 54.27
(a) The density of the gas as a function of z (the cylindrical axis) for five different radii uniformly spaced inside the target hole. The origin is at the target center. The density is relative to the density of gas backing the device. (b) The distribution of gas particles in the target as a function of radius ($z = 0$) from the target center out to the inside edge of the gas pocket ($r = 4$ mm), where the density is assigned a value of 1. The target hole's cylindrical wall is at $r = 0.25$ mm.

Calculation of Gas Density within the Gas Target

The gas distribution in a target has been calculated using the Monte Carlo computer simulation of free molecular flow described in the previous section. The dimensions of the target in the simulation were $a = 0.2$ mm, $c = 0.4$ mm, $d = 0.5$ mm, and $L = 4$ mm (see Fig. 54.27). The number of particles propagated through the system was such that 10,000 successfully exited the hole. The throughput probability for an individual particle was 0.014, which later will be used to find the gas-flow rate. This small number indicates that very few particles entering the system actually exit the target opening before returning to the starting point (1 in 70). This can be understood in part by the relative sizes of the

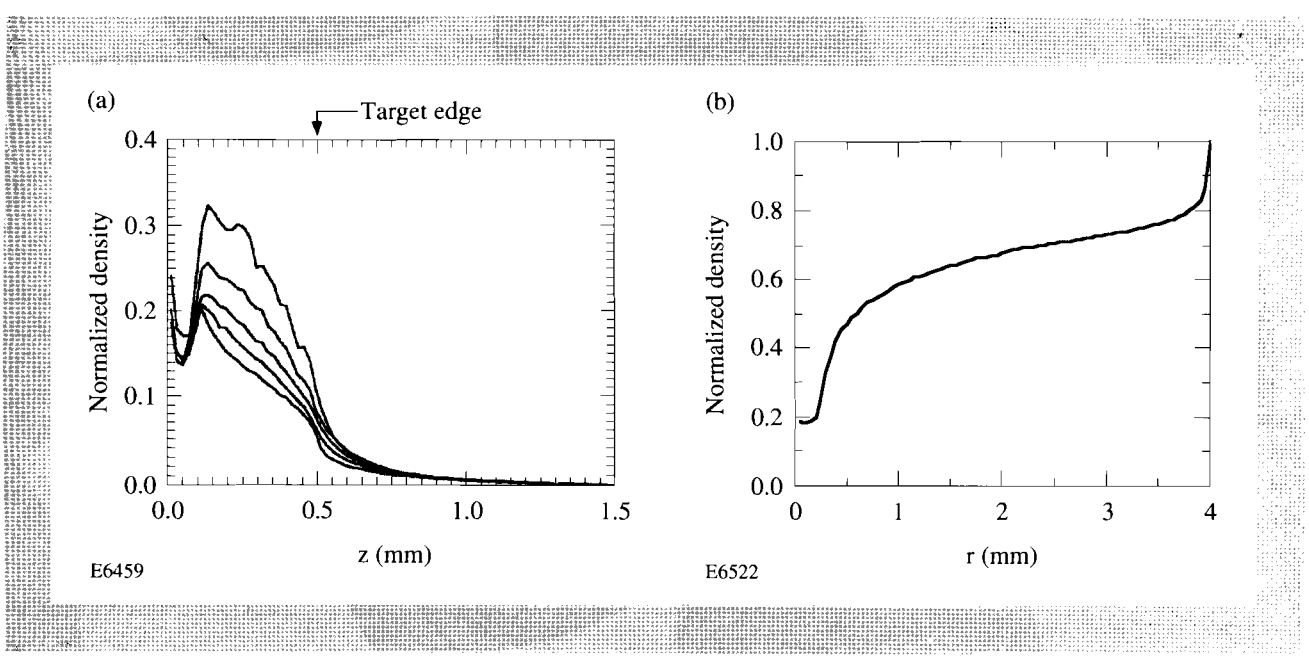

entrance and exit areas (a factor-of-16 difference). Figure 54.27(a) shows the density of the gas as a function of z (the cylindrical axis) for five different radii uniformly spaced inside the center hole. The density is normalized to the density at the inside edge of the ring-shaped gas pocket (length L from the center), where the backing pressure is known. As can be seen, the density is only weakly dependent on radius. Along the z axis, the density falls off sharply at the edge of the hole (located at 0.5 mm). The reason for this sharp drop is that the particles within the hole tend to have a strong radial component to their velocity so that when they exit the hole into the free vacuum, they quickly spread away from the z axis. Figure 54.27(b) shows the particle density as a function of radius for $z = 0$. Again the density is normalized to that in the ring-shaped pocket, so that at a radius of 4 mm (the boundary with the pocket) the density is 1. From there, the density continually drops until inside the target opening ($r < 0.25$ mm), where the density on average is ~0.2.

Gas-Flow Rate

The flow rate of gas through the target can be derived from the throughput probability calculated using the Monte Carlo technique previously described. The number of particles that exit the nozzle per time is

$$\dot{N} = \rho(A\delta)\left(\frac{v_{mf}}{4\delta}\right)\gamma , \tag{6}$$

where ρ is the backing particle density, A is the entrance area at the edge of the ring-shaped gas pocket ($2\pi aL$), v_{mf} is the mean-free velocity of the particles, and γ is the throughput probability. Introduced here briefly for conceptual convenience, δ is a small thickness that when multiplied onto the entrance area creates an element of volume. The factor of 4 in the denominator comes about since only half the particles within the volume element are moving in a direction that will take them into the plates, and their component of velocity normal to the entrance is on average one-half the mean-free velocity. Replacing ρ by N/V, where V is the fixed backing volume, and solving the differential equation yields

$$N = N_0 \exp\left\{-\frac{A\gamma v_{mf}}{4V}t\right\} . \tag{7}$$

Since pressure is proportional to the number of particles, Eq. (7) applies as well to pressure. A useful term for comparison with experimental measurement is the time it takes for the pressure to drop by a factor of 2. The half-life of the pressure is

$$t_{\text{half}} = \frac{4\ln 2V}{\gamma A v_{mf}} . \tag{8}$$

This theoretical result can be compared with experimental measurements as a check of the model.

A gas target with the same dimensions as used in the numerical simulations has been tested. The half-lives of the backing pressure in our system predicted by Eq. (8) for He, Ar, and Xe were 6 s, 19 s, and 35 s, respectively; we measured 9 s, 25 s, and 45 s. The measurements were taken at the pressures where the molecular flow range was expected to begin for the various gases. The backing pressures were 1 Torr, 0.5 Torr, and 0.3 Torr, respectively. Recall that the pressure at the target center is a factor of 5 below the backing pressure (see Fig. 54.27). For each gas, the flow rate approximately doubled when four times the backing pressure was applied. Higher backing pressures produced faster flow rates since intraparticle collisions began to reduce the randomness to the direction in which the particles drifted through the target. However, these pressures were still very far below the viscous flow regime. At lower pressures, the gas flow slowed because the walls and tubes in our backing system began to play a significant role.

To further test the accuracy of the model, a different gas target with the dimensions of $a = 0.12$ mm, $c = 0.17$ mm, $d = 0.35$ mm, and $L = 3.0$ mm (see Fig. 54.26) was tested. The calculated throughput probability was 0.013, which for our system predicted a pressure half-life of 43 s for Ar; the measured half-life was 35 s. The good agreement between predicted and measured flow rates lends confidence to the accuracy of the model.

Sensitivity of Gas Flow and Density to the Nature of the Surfaces

The question arises—how sensitive is the flow of gas in the target to the material nature of the walls. In other words, how good is the assumption that the particles rebound from the walls of the target with a Lambertian distribution. To answer the question, the Monte Carlo simulation was modified to allow a fraction of the particle-surface rebounds to be specular or mirror-like. For a specular reflection with the planar surface, the new slopes, rather than those of Eq. (1), are given simply by $m_x' = -m_x$ and $m_y' = -m_y$. For a specular reflection off the interior surface of the cylindrical hole, the new slopes, rather than those of Eq. (5), are given as $m_x' = \left(2\sin^2\phi - 1\right)m_x - \sin(2\phi)m_y$ and $m_y' = -\sin(2\phi)m_x - \left(2\sin^2\phi - 1\right)m_y$. The Monte Carlo simulations with up to half the interior particle-surface collisions treated as specular reflections showed that there is very little effect on the gas distribution except for an increase in the gas-flow rate (40%). The model therefore seems only mildly sensitive to the nature of the surfaces.

Experimental Measurement of Gas Density

The gas distribution for a target with the same dimensions as previously described ($a = 0.2$ mm, $c = 0.4$ mm, $d = 0.5$ mm, and $L = 4$ mm) was measured. The distribution of gas from the target opening out into the region in front is characterized using a 45°-off-axis imaging system that observes the recombination light from laser-induced ionization of Xe. The imaging system employs a lens, a slit, and a photomultiplier tube, which observes recombination light from a ~500-μm section of the laser beam. The gas target is positioned at various distances away from the location. Figure 54.28 shows the experimental setup for the measurement. The laser beam was a 1-μm, 1-ps pulse focused with *f*/70 optics to a peak intensity of 2×10^{14} W/cm^2. Figure 54.29 shows the effect of the spatial

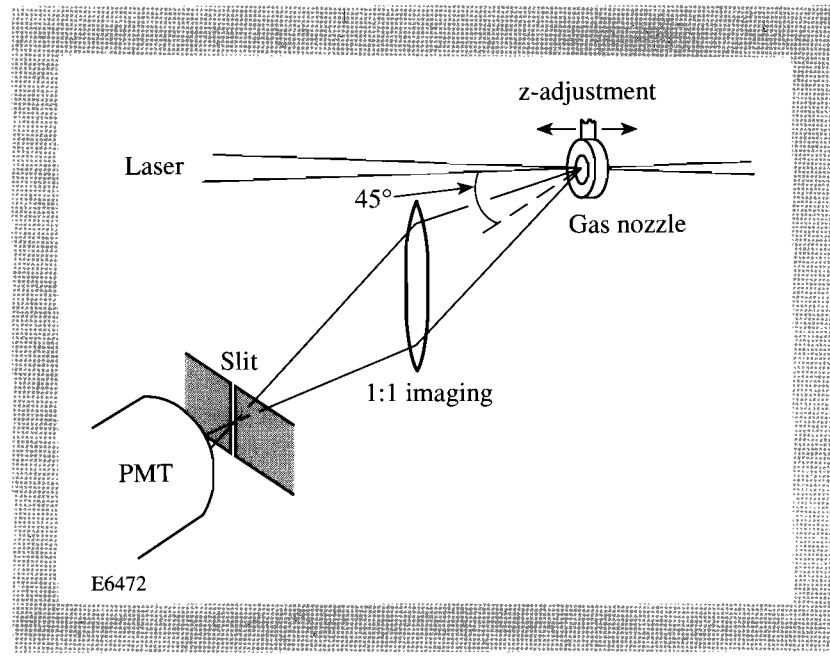

Fig. 54.28
The experimental setup for measuring the gas density just inside the target opening and outward along the z axis.

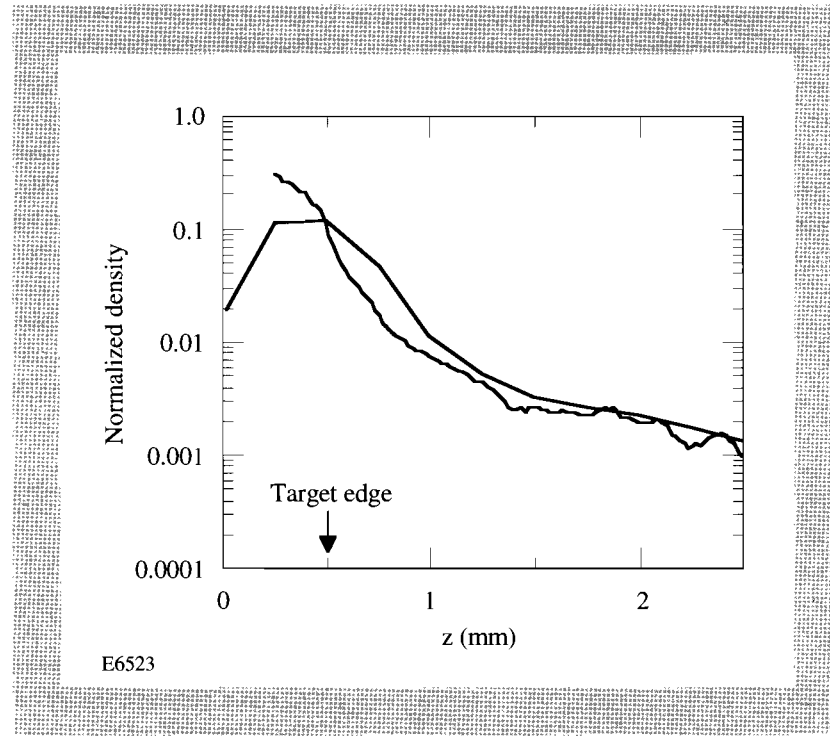

Fig. 54.29
The calculated density of the gas as a function of z along the cylindrical axis [see Fig. 54.27(a)] compared with its convolution with the detector resolution.

resolution of the detection scheme on the calculated density. The figure shows the axial gas distribution taken from Fig. 54.27(a) along with its convolution with the experimental resolution. The measured gas density must be compared to this convolved curve to assess agreement with the calculated density.

The experimental results agree well with the theoretical predictions, especially at lower pressures. Figure 54.30 shows a comparison in absolute pressure between the predicted and measured gas density for a backing pressure of 1.7 Torr. Again, it should be noted that the results are convolved by the experimental resolution. As seen in Fig. 54.29, this causes the peak density to appear a factor of 2 below the actual value. The density was normalized by comparing the results to the signal obtained when back-filling the vacuum chamber (target removed) to a known pressure (0.1 Torr). A low pressure had to be used for calibration to avoid significant refraction of the laser before it arrived to the imaged position. It was assumed that the gas density was proportional to the square root of the instantaneous (time scale of the order of tens of nanoseconds) recombination signal.[9]

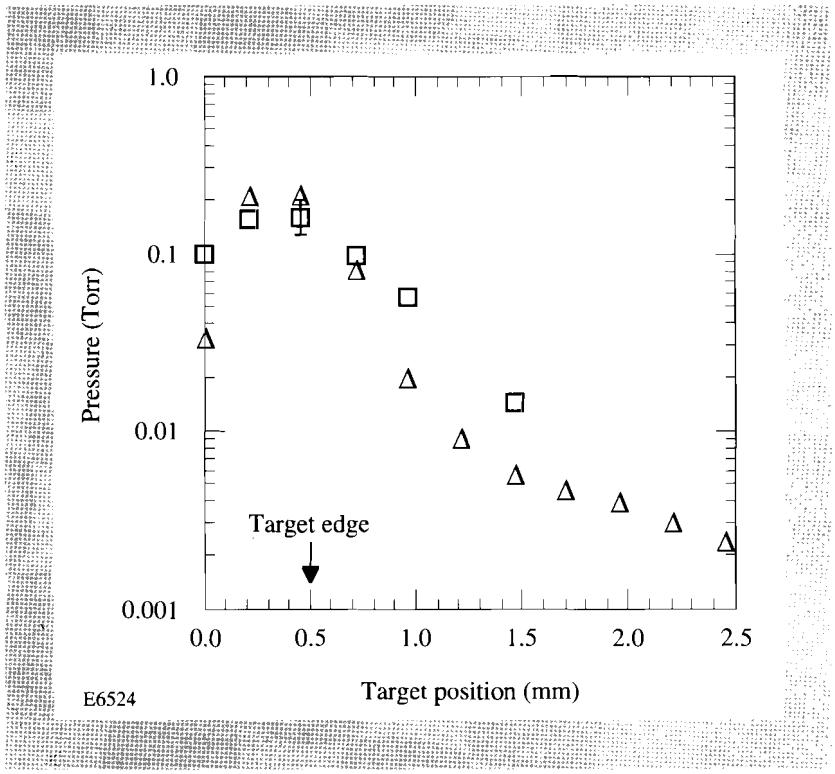

Fig. 54.30
A comparison between the predicted- and measured-gas-density profiles for a backing pressure of 1.7 Torr.

Figure 54.31 shows the results obtained for a wide variety of backing pressures. The gas density decreases rapidly outside the target hole along the laser axis even for pressures up to ten times the molecular-flow-range cutoff. In the molecular-flow range (backing pressure of 0.5 Torr), the gas density fell by more than a factor of 10 at a distance of 1 mm from the target opening. With backing pressures of 3 Torr and 10 Torr applied to the target, the density dropped by a factor of 10 and 5, respectively, at 1 mm. These comparisons neglected the convolution effect of the experimental resolution. Inclusion of this effect

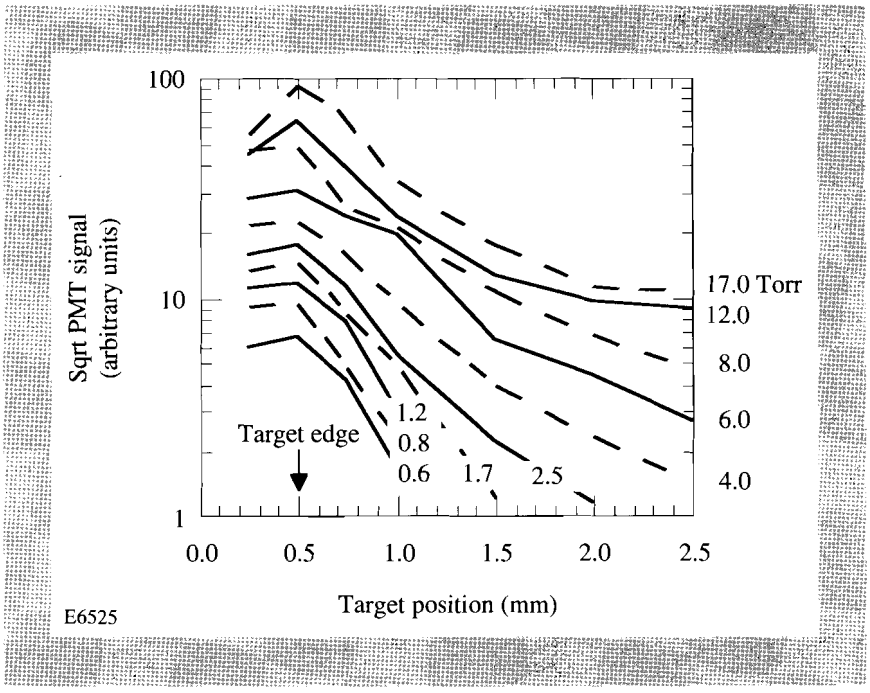

Fig. 54.31
The measured density of the gas as a function of z (the cylindrical axis) for ten different backing pressures: 0.6, 0.8, 1.2, 1.7, 2.5, 4, 6, 8, 12, and 17 Torr.

improves the contrast by about a factor of 2. The experiment thus shows that the gas target is capable of exceeding the molecular-flow regime to Kn as low as 0.1 without serious distortion of the gas distribution. It was also found that over this range of pressure the density in the target hole scales roughly with the backing pressure. Figure 54.32 shows the measured density in the target opening plotted against the backing pressure. On the log-log plot, the points should follow a slope of 1 for them to behave like pure molecular flow. The deviation from a slope of 1 shows that the gas-density profile may have a slight pressure dependence with the target operating above the molecular-flow range.

Summary

A gas target for use in laser-atom harmonic-generation experiments has been developed. It consists of a small, cylindrical, double-ended hole through which the laser passes. Gas enters the hole along the center of its cylindrical wall and quickly disperses as it emerges out either end of the hole. The target is able to produce a narrow, low-density gas distribution that can be easily intersected by a focused laser. The distribution is well characterized both theoretically and experimentally. Recently, the target has been employed successfully in high-harmonic-generation experiments. The low-density, narrow profile of the gas is advantageous in reducing the role of phase matching and refraction in the experiment.[10]

To date, harmonic-generation experiments have typically employed a pulsed gas jet. The gas jet relies on the principles of viscous flow to propel gas from the orifice in a thin stream where a laser can intersect with the narrow distribution of gas. In contrast, the gas target relies on the principles of molecular flow to disperse the gas quickly once outside the central hole. Both systems are restricted to operating in their respective flow regimes to ensure the narrowest-possible gas distribution. The two systems are thus complementary in the sense that they operate in opposite pressure ranges.

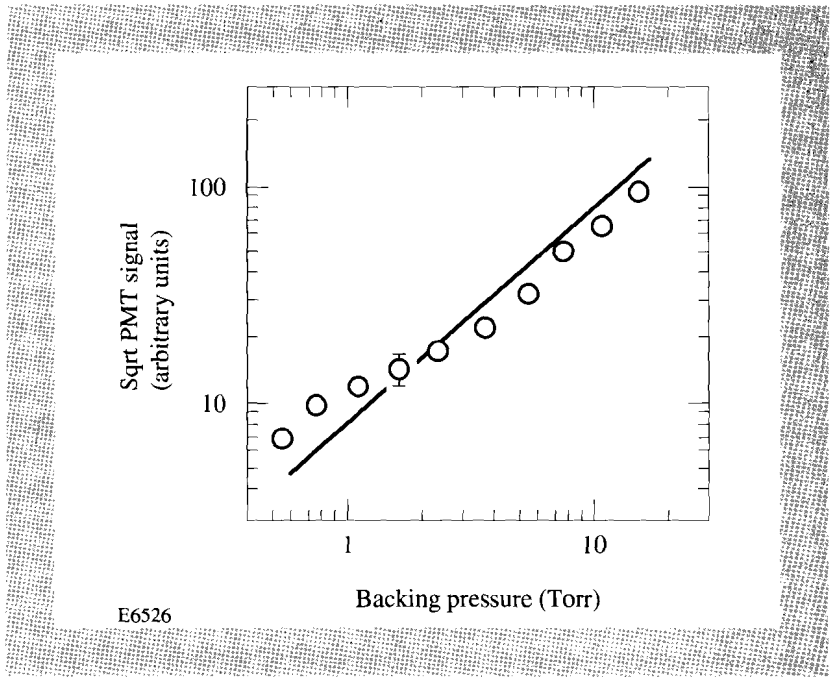

Fig. 54.32
The measured density in the target opening plotted against the backing pressure. The solid line, shown for comparison, has a slope of 1.

ACKNOWLEDGMENT

This work is supported by the National Science Foundation under contract PHY-9200542. Additional support was provided by the U.S. Department of Energy Office of Inertial Confinement Fusion under Cooperative Agreement No. DE-FC03-92SF19460 and the University of Rochester. The support of DOE does not constitute an endorsement by the DOE of the views expressed in this article.

REFERENCES

1. A. L'Huillier, K. J. Schafer, and K. C. Kulander, J. Phys. B **24**, 3315 (1991).
2. A. L'Huillier, K. J. Schafer, and K. C. Kulander, Phys. Rev. Lett. **66**, 2200 (1991).
3. Ph. Balcou and A. L'Huillier, to be published in *Physical Review A*.
4. J. F. Reintjes, *Nonlinear Optical Parametric Processes in Liquids and Gases* (Academic Press, New York, 1984).
5. A. McPherson *et al.*, J. Opt. Soc. Am. B **4**, 595 (1987).
6. L. A. Lompré *et al.*, J. Appl. Phys. **63**, 1791 (1988).
7. G. A. Bird, *Molecular Gas Dynamics* (Clarendon Press, Oxford, 1976).
8. J. F. O'Hanlon, *A User's Guide to Vacuum Technology* (Wiley, New York, 1980).
9. H. R. Griem, *Plasma Spectroscopy* (McGraw-Hill, New York, 1964).
10. D. D. Meyerhofer and J. Peatross, "Angular Distributions of High-Order Harmonics," to be published in the *Proceedings of the NATO Workshop on Super-Intense, Laser-Atom Physics*, edited by B. Piraux, Han-sur-Lesse, Belgium, 8–14 January 1993.